Direct probing of photoinduced electron transfer in a self- assembled biomimetic [2Fe2S]-hydrogenase complex using ultrafast vibrational spectroscopy

Inorganic Chemistry

Article

pubs.acs.org/IC

Direct Probing of Photoinduced Electron Transfer in a Self-Assembled Biomimetic [2Fe2S]-Hydrogenase Complex Using Ultrafast Vibrational Spectroscopy

Ping Li,[†,⊥] Saeed Amirjalayer,[‡,⊥] František Hartl,*[,§] Martin Lutz,[∥] Bas de Bruin,[†] René Becker,[†] Sander Woutersen,*[,‡] and Joost N. H. Reek*[,†]

[†]Homogeneous & Supramolecular Catalysis, van 't Hoff Institute for Molecular Sciences, University of Amsterdam, Science Park 904, 1098 XH Amsterdam, The Netherlands

[‡]Molecular Photonics, van 't Hoff Institute for Molecular Sciences, University of Amsterdam, Science Park 904, 1098 XH Amsterdam, The Netherlands

[§]Department of Chemistry, University of Reading, Whiteknights, Reading RG6 6AD, United Kingdom

[∥]Crystal and Structural Chemistry, Bijvoet Center for Biomolecular Research, Utrecht University, Padualaan 8, 3584 CH Utrecht, The Netherlands

Supporting Information

ABSTRACT: A pyridyl-functionalized diiron dithiolate complex, [μ-(4-pyCH_2−NMI-S_2)$Fe_2(CO)_6$] (**3**, py = pyridine (ligand), NMI = naphthalene monoimide) was synthesized and fully characterized. In the presence of zinc tetraphenylporphyrin (ZnTPP), a self-assembled **3**·ZnTPP complex was readily formed in CH_2Cl_2 by the coordination of the pyridyl nitrogen to the porphyrin zinc center. Ultrafast photoinduced electron transfer from excited ZnTPP to complex **3** in the supramolecular assembly was observed in real time by monitoring the ν(C≡O) and $\nu(C{=}O)_{NMI}$ spectral changes with femtosecond time-resolved infrared (TRIR) spectroscopy. We have confirmed that photoinduced charge separation produced the monoreduced species by comparing the time-resolved IR spectra with the conventional IR spectra of $\mathbf{3}^{\bullet-}$ generated by reversible electrochemical reduction. The lifetimes for the charge separation and charge recombination processes were found to be τ_{CS} = 40 ± 3 ps and τ_{CR} = 205 ± 14 ps, respectively. The charge recombination is much slower than that in an analogous *covalent* complex, demonstrating the potential of a supramolecular approach to extend the lifetime of the charge-separated state in photocatalytic complexes. The observed vibrational frequency shifts provide a very sensitive probe of the delocalization of the electron-spin density over the different parts of the Fe_2S_2 complex. The TR and spectro-electrochemical IR spectra, electron paramagnetic resonance spectra, and density functional theory calculations all show that the spin density in $\mathbf{3}^{\bullet-}$ is delocalized over the diiron core and the NMI bridge. This delocalization explains why the complex exhibits low catalytic dihydrogen production even though it features a very efficient photoinduced electron transfer. The ultrafast porphyrin-to-NMI-S_2−$Fe_2(CO)_6$ photoinduced electron transfer is the first reported example of a supramolecular Fe_2S_2-hydrogenase model studied by femtosecond TRIR spectroscopy. Our results show that TRIR spectroscopy is a powerful tool to investigate photoinduced electron transfer in potential dihydrogen-producing catalytic complexes, and that way to optimize their performance by rational approaches.

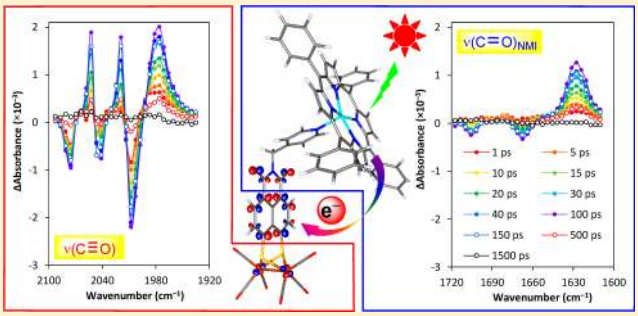

INTRODUCTION

Artificial mimics of the active site of [FeFe]-hydrogenases have attracted increasing attention in the past 15 years,[1] since the enzyme structure was deduced from X-ray crystallography.[2] To date, hundreds of diiron dithiolate model complexes have been explored as electroactive catalysts for proton reduction along homo- or heterogeneous catalytic paths.[3] More recently, photocatalytic hydrogen production based on Fe_2S_2 complexes in a combination with a light-harvesting chromophore has been demonstrated.[4] Three strategies have been developed to achieve effective electronic communication between the chromophore and the catalytic site, namely, (a) covalent linkage, (b) multicomponent systems, and (c) supramolecular assemblies. Quenching of the excited state in the first family of covalently bound Ru(terpy)$_2$-Fe_2S_2 systems was attributed to fast energy transfer.[5,6] Moreover, a reductive quenching by the electron-rich diiron center was encountered for the Ru^{2+}

Received: April 3, 2014
Published: April 26, 2014

   dx.doi.org/10.1021/ic500777d | *Inorg. Chem.* 2014, 53, 5373−5383

Chart 1. Schematic Molecular Structures of Selected Diiron Hydrogenase Model Complexes

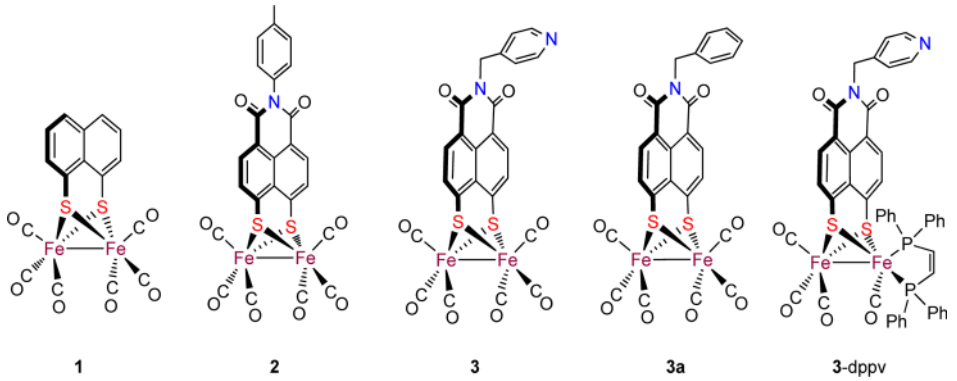

photosensitizer side-attached via a phosphine ligand.[7] In contrast, an intermolecular electron transfer from photo reduced $[Ru(bpy)_3]^+$ to $[(\mu\text{-}SCH_2)_2XFe_2(CO)_6]$ (X = CH_2 or NCH_2Ph) was proven with transient absorption (TA) spectroscopy.[8] More recently, the formation of a Fe^0Fe^I species via one-electron transfer from the photogenerated organic radical, $Et_2N\dot{C}HCH_3$, to $[(\mu\text{-pdt})Fe_2(CO)_5(PMe_3)]$ (pdt = propane-1,3-dithiolate), was confirmed by quenching experiments monitored *in situ* by electron paramagnetic resonance (EPR) spectroscopy.[9]

The first example of a self-assembled porphyrin-diiron complex, namely, $[(\mu\text{-}SCH_2)_2NC(O)C_5H_4N]Fe_2(CO)_6$·ZnTPP, was reported by Song and co-workers.[10] A luminescence quenching efficiency up to 78% within this self-assembly supported the proposed electron transfer. Two years later, the first evidence from time-resolved (TR) spectroscopy was obtained for the electron transfer from excited ZnTPP to $[\{(\mu\text{-}SCH_2)_2N(CH_2CH_2OOCPy)\}Fe_2(CO)_6]$ in a noncovalent assembly. The diiron core photoreduction was verified by using nanosecond flash photolysis in the Sun's laboratory.[11] Shortly afterward, our group reported a family of self-assembled Fe_2S_2−PPh_2(pyridyl)-zinc porphyrin complexes that exhibited photocatalytic activity, notably in the presence of two different porphyrin chromophores. Infrared (IR) spectroscopic monitoring of the photoreaction has revealed that a disubstituted catalyst, namely, $[(\mu\text{-pdt})Fe_2(CO)_4(PPh_2Py)_2]$, was formed via disproportionation of the photo reduced parent pentacarbonyl complex.[12]

More recently, a photodriven ultrafast intramolecular electron transfer from photoexcited zinc porphyrin to a hydrogenase-model diiron dithiolate complex was thoroughly investigated by Wasielewski and co-workers in covalently linked zinc porphyrin-NMI-S_2−$Fe_2(CO)_6$ (NMI = naphthalene monoimide) with femtosecond TA spectroscopy.[13] The study yielded lifetimes for the charge separation and recombination processes, namely, τ_{CS} = 24 ± 1 ps and τ_{CR} = 57 ± 1 ps (CH_2Cl_2), respectively. Compared to the NMI-lacking reference complex, that is, $[(\mu\text{-naphdt})Fe_2(CO)_6]$ (**1**, naphdt = naphthalene-1,8-dithiolate)[14] (Chart 1), the incorporation of the electron-withdrawing NMI group in $[\mu\text{-(tol-NMI-}S_2)\text{-}Fe_2(CO)_6]$ (tol = toluene) (**2**; Chart 1) positively shifted the first reduction potential by *ca.* 0.4 V and made the electron transfer from zinc porphyrin (ZnP) to the diiron part in **2**-ZnP thermodynamically favorable (ΔG = −0.63 V).[13a] Notably, the charge recombination process slowed down to τ_{CR} = 67 ± 2 ns by incorporating a ferrocenyl (Fc) substituent on a phenyl group of ZnTPP, leading to a subsequent second electron transfer from Fc to $ZnTPP^{\bullet+}$.[13b] These reports have introduced an ideal model system to study the ultrafast electron transfer process closely related to photocatalytic dihydrogen production. However, the formation of the reduced diiron dithiolate species was only monitored by transient electronic absorption with a maximum at 616 nm, most likely corresponding to the reduced NMI-S_2−$Fe^0Fe^I(CO)_6$ species.

On the other hand, IR spectroscopy has been established as a powerful tool for the direct characterization of active intermediates formed during electrochemical redox reactions and protonation of diiron dithiolate complexes in the ground state,[15] that is, without photoexcitation of a light harvesting chromophore component in the assembly, benefiting from the high sensitivity of C≡O stretching modes to changes in the π-back-donation from the substituted diiron core. For example, a mixed-valence paramagnetic Fe^IFe^{II} hydride-bridged species has recently been characterized by IR spectroelectrochemistry.[16] To obtain a detailed understanding of photoinduced electron transfer in potential dihydrogen-producing catalytic complexes, one ideally would like to combine the high sensitivity of the IR response with the subpicosecond time resolution that has already been achieved in the visible wavelength region. To the best of our knowledge, the electron transfer process from a photoexcited chromophore to a diiron hydrogenase model complex has yet not been investigated by transient IR spectroscopy (TRIR). Here we report such an ultrafast TRIR spectroscopic study of photoinduced electron transfer in a self-assembled Fe_2S_2·ZnTPP system, Fe_2S_2 standing for $[\mu\text{-(4-py}CH_2\text{−NMI-}S_2)Fe_2(CO)_6]$ (**3**, Chart 1), wherein the ZnTPP chromophore in the selectively populated singlet excited state transfers an electron to the Fe_2S_2 complex unit. The photo reduced species, $\mathbf{3}^{\bullet-}$, was also characterized separately by IR and ultraviolet−visible (UV−vis) spectroelectrochemistry, EPR spectroscopy and density functional theory (DFT) calculations. Furthermore, we investigated the influence of carbonyl substitution at the diiron center on its redox properties with $[\mu\text{-(4-py}CH_2\text{−NMI-}S_2)Fe_2(CO)_4(dppv)]$ (**3**-dppv, dppv = *cis*-1,2-bis(diphenylphosphino)ethylene; Chart 1). This study shows for the first time by TRIR the rate of electron transfer from the photoexcited state of the chromophore to the [FeFe]-Hydrogenase model complex, and that the spin density is located mainly on the organic NMI ligand rather than on the metal, thereby explaining the adverse effect on the light-driven proton reduction.

dx.doi.org/10.1021/ic500777d | *Inorg. Chem.* 2014, 53, 5373−5383

RESULTS AND DISCUSSION

Self-Assembly Study of 3·ZnTPP. Pyridin-4-yl-functionalized complex **3** was readily prepared in a moderate yield (50%) by treating the disulfide ligand, 4-pyCH$_2$−NMI-S$_2$ (**L**, see Supporting Information, Figure S1 for its X-ray crystal structure), with 2 equiv of [Fe$_2$(CO)$_9$] in tetrahydrofuran (THF) at room temperature (RT) for 2 h. Complex **3** was fully characterized by ^{1}H NMR, Fourier transform (FT) IR spectroscopies, high-resolution mass spectrometry (HR-MS), and X-ray crystal structure determination (Figure 1). In

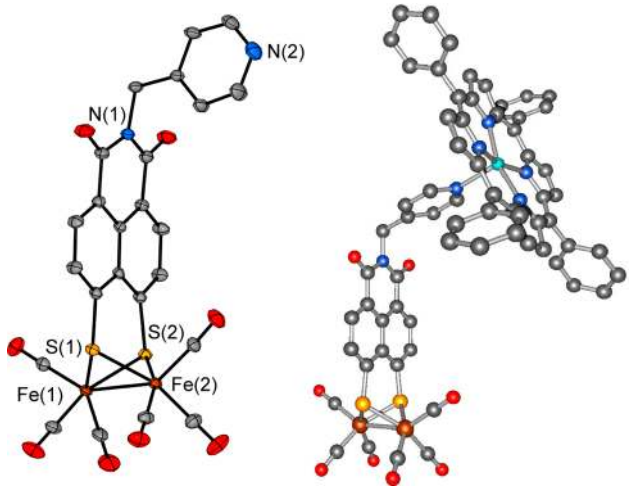

Figure 1. (left) Molecular structure of [(4-pyCH$_2$−NMI-S$_2$)-Fe$_2$(CO)$_6$] (**3**) in the crystal, with displacement ellipsoids drawn at the 50% probability level. Hydrogen atoms are omitted for clarity. Selected bond lengths (Å), angles (deg) and torsion angles (deg): Fe(1)−Fe(2), 2.50955(16); Fe(1)−S(1), 2.2361(2); Fe(1)−S(2), 2.2442(2); Fe(2)−S(1), 2.2402(2); Fe(2)−S(2), 2.2451(2); Fe(1)−CO$_{ap}$, 1.7894(8); Fe(1)−CO$_{ba}$, 1.8057(9); Fe(2)−CO$_{ap}$, 1.7993(10); Fe(2)−CO$_{ba}$, 1.8024(8); S(1)−Fe(1)−S(2), 85.225(8); S(1)−Fe(2)−S(2), 85.107(8); S(1)−Fe(1)−Fe(2)−S(2), −109.494(9). (right) DFT-optimized (BP86, def2-TZVP) structure of self-assembled **3**·ZnTPP.

CH_2Cl_2, complex **3** exhibits three characteristic ν(C≡O) bands at 2080, 2046, and 2007 cm^{-1} (Supporting Information, Figure S2), which are blue-shifted by *ca.* 2 cm^{-1} compared to [μ-(tol-NMI-S$_2$)Fe$_2$(CO)$_6$] (**2**; Chart 1).[13] Two additional weak absorption bands are found at 1706 and 1664 cm^{-1} belonging to ν(C═O)$_{NMI}$ vibrations of the monoimide carbonyls. Similar wavenumbers, namely, 1691 and 1653 cm^{-1}, were also observed for free ligand **L** in CH_2Cl_2 (Supporting Information, Figure S2). The single-crystal X-ray structure determination revealed the characteristic butterfly Fe$_2$S$_2$ core of **3** featuring an Fe−Fe bond length of 2.50955(16) Å.

To study the self-assembling process between complex **3** and ZnTPP in solution, steady-state UV−vis and emission spectra were recorded during the titration of 8.0 × 10^{-5} mol dm^{-3} ZnTPP in CH_2Cl_2 by complex **3**. An apparent red shift of the Q-bands of ZnTPP was observed upon the addition of complex **3** (Supporting Information, Figure S3), reflecting the axial coordination of the pyridyl-N to the porphyrin zinc center. The determined association constant K_{ass} = 4.5 × 10^3 mol^{-1} dm^3 is comparable with those for the related examples.[11,12] The titration of ZnTPP with the free disulfide ligand (**L**) was accompanied by similar red shift of Q-bands with a well-defined isosbestic point at 555 nm and gave the association constant K_{ass} = 1.2 × 10^4 mol^{-1} dm^3 (Supporting Information, Figure S4).

As shown in Figure 2, the luminescence of ZnTPP at 598 and 644 nm was strongly quenched (up to 87%) upon addition of

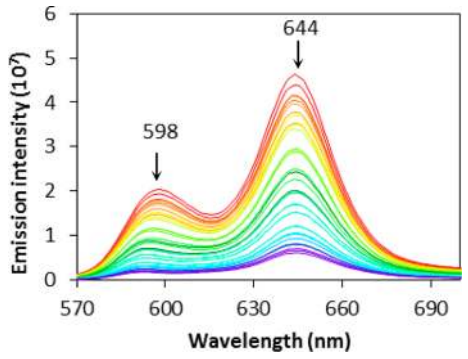

Figure 2. Luminescence quenching observed along the titration of ZnTPP with [μ-(4-pyCH$_2$−NMI-S$_2$)Fe$_2$(CO)$_6$] (**3**) in CH_2Cl_2. Excitation wavelength: 555 nm. Concentrations: [ZnTPP] = 8.0 × 10^{-5} mol dm^{-3}; [**3**] = 0 (red) to *ca.* 1.0 × 10^{-3} mol dm^{-3} (purple).

ca. 13 equiv of complex **3** to the ZnTPP solution in CH_2Cl_2. The Stern−Volmer constant K_{SV} = 6.2 × 10^3 mol^{-1} dm^3 was calculated from the linear dependence of $F(0)/F$ (emission intensity before/after the addition of the quencher) on the concentration of **3** in the corresponding Stern−Volmer plot (Supporting Information, Figure S5). In a control experiment using a pyridyl-free compound, [μ-(PhCH$_2$−NMI-S$_2$)-Fe$_2$(CO)$_6$] (**3a**), instead of **3**, a much smaller Stern−Volmer constant K_{SV} = 9.2 × 10^2 mol^{-1} dm^3 was observed (Supporting Information, Figure S6), the small residual quenching most likely being due to occasional complexation (probably mediated by π-stacking) between **3a** and ZnTPP.

Time-Resolved Infrared Spectroscopy, Infrared Spectroelectrochemistry, and DFT Calculations. Complex **3** in CH_2Cl_2 displays two reversible one-electron reduction steps at $E_{1/2}$ = −1.28 and −1.65 V (vs Fc/Fc$^+$, Supporting Information, Figure S7). The cathodic potentials are negatively shifted by *ca.* 0.14 V compared to the values reported for [μ-(tol-NMI-S$_2$)Fe$_2$(CO)$_6$] (**2**).[13a] In the DFT-optimized self-assembled **3**·ZnTPP (see Supporting Information, Figure S8 for frontier orbitals), the driving force for the photodriven electron transfer from photoexcited ^{1}ZnTPP to complex **3** has been estimated as $-\Delta G_{CS}$ = 0.64 eV in CH_2Cl_2 (see the Supporting Information), indicating that the charge separation is thermodynamically feasible.

A femtosecond-to-picosecond TRIR study was conducted with 2.0 mM **3** and 2.0 mM ZnTPP in CH_2Cl_2, wherein the concentration of the dynamic self-assembly, **3**·ZnTPP, is *ca.* 1.4 mol dm^{-3} according to the association constant calculated above. ZnTPP was selectively photoexcited by a 553 nm laser pulse. The difference absorbance transient IR spectra recorded in the ν(C≡O) and ν(C═O)$_{NMI}$ regions are shown in Figure 3a,b, respectively. The time resolution of the experiment was ∼200 fs.

Photodriven ultrafast electron transfer from excited ^{1}ZnTPP to complex **3** resulted in the gradual formation of one-electron reduced **3**$^{\bullet-}$ (characterized separately by IR spectroelectrochemistry, see below). As shown in Figure 3a, the three positive ν(C≡O) bands around 2052, 2019, and 1976 cm^{-1} of **3**$^{\bullet-}$

dx.doi.org/10.1021/ic500777d | Inorg. Chem. 2014, 53, 5373−5383

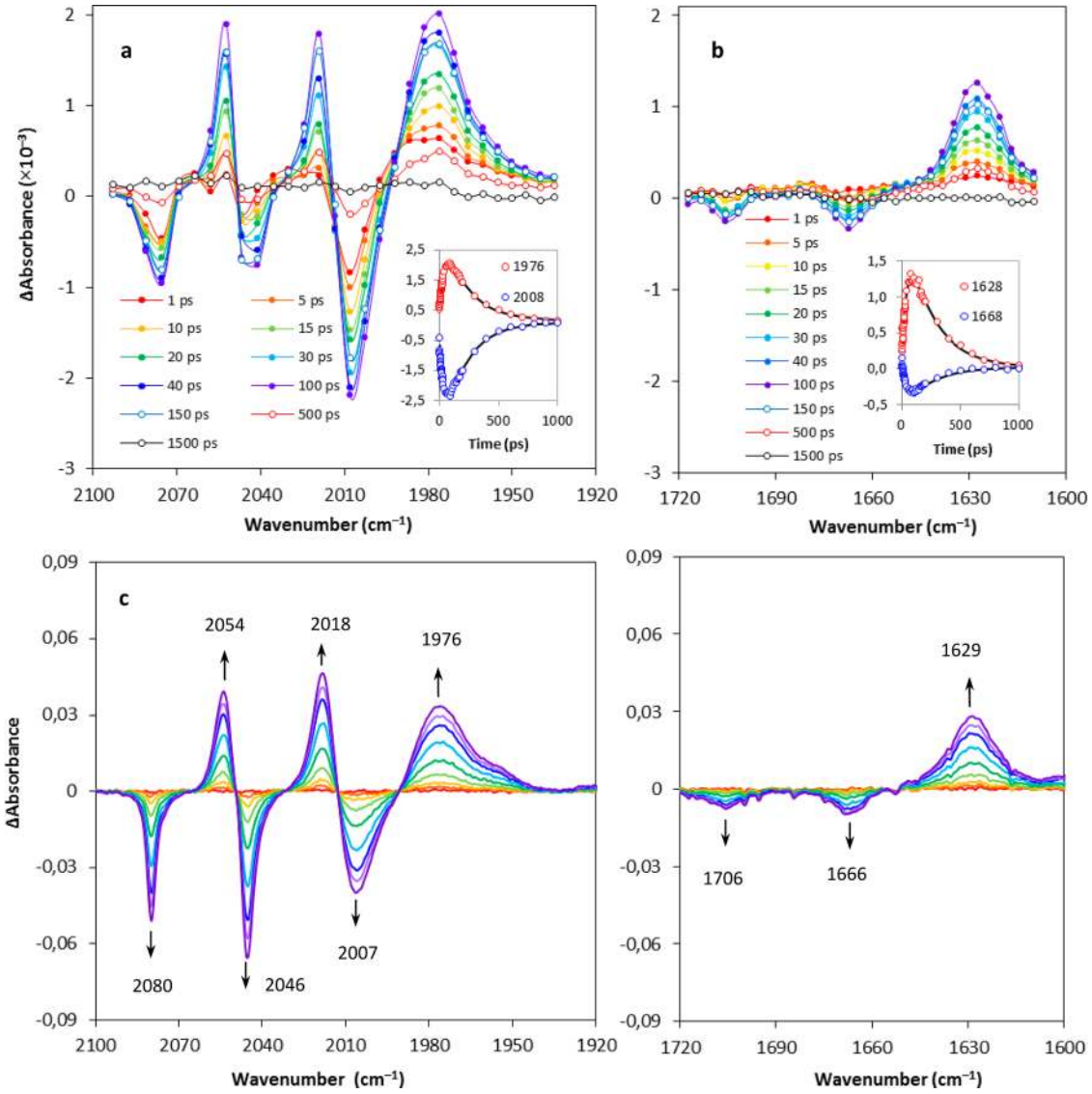

Figure 3. (top) TRIR spectra recorded in different wavenumber regions (a) ν(C≡O) and (b) $\nu(C{=}O)_{NMI}$ for 2.0 mM [μ-(4-pyCH_2−NMI-S_2)$Fe_2(CO)_6$] (**3**) and 2.0 mM ZnTPP in CH_2Cl_2 at 293 K, following the 553 nm fs laser excitation. The insets show the corresponding kinetic traces at 1976 and 2008 cm^{-1} (a), and at 1628 and 1668 cm^{-1} (b), respectively. The curves through the data points are the result of a global least-squares fit. (bottom) Absorbance difference IR SEC spectra recorded in different wavenumber regions (c) ν(C≡O) and (d) $\nu(C{=}O)_{NMI}$ during the one-electron reduction of 1.0 mM **3** in CH_2Cl_2 (0.1 M nBu$_4$NPF$_6$) within an OTTLE cell at 293 K (see Supporting Information, Figure S9 for the thin-layer cyclic voltammogram response).

arose simultaneously with the bleaching of the ground state absorption of the parent compound around 2075, 2044, and 2008 cm^{-1}. The IR pattern remained as three well-defined peaks after the charge separation, indicating that no significant geometry change occurred at the diiron dithiolate hexacarbonyl moiety during its photo reduction. The maximum ground state bleach was achieved in *ca.* 100 ps, followed by the decay of the charge separated state. The zero absorbance line was restored within 1.5 ns, indicating that the ground state was fully recovered by the charge recombination. Global kinetics curve fitting yielded the lifetimes for the charge separation and charge recombination as τ_{CS} = 40 ± 3 ps and τ_{CR} = 205 ± 14 ps, respectively. Compared to the covalently bonded model **2**-ZnP,[13a] both processes, but in particular the charge recombination (from 57 to 205 ps), were significantly slowed down in **3**·ZnTPP, which was most likely caused by two effects: (1) the bond distance between the photosensitizer and acceptor is different, because of the additional methylene linker; (2) the relative orientations of the photosensitizer and the electron acceptor are significantly different in the covalently linked and supramolecular complex. In **2**-ZnP, the porphyrin ring is approximately parallel to the NMI symmetry axis, whereas in **3**·ZnTPP it is at an angle of ∼22°. Both the distance and the relative orientation of the electron donor and acceptor have a strong influence on the electron-transfer rate. Additionally, the coordination sphere of the zinc atom is different in the two structures as the coordination number of Zn changed from 4 to 5 due to axial coordination of the pyridine in **3**·ZnTPP, which could also change the driving force for the electron transfer. To test the influence of the axial-pyridine ligand on the redox potentials of ZnTPP, cyclic voltammetry of ZnTPP (1.0 mM) was conducted in the absence and presence of 4-ethylpyridine (10 mM; see Supporting Information, Figure S10). The energy level analysis (Supporting Information,

dx.doi.org/10.1021/ic500777d | *Inorg. Chem.* 2014, 53, 5373−5383

Figure S11) revealed that the coordination of the pyridine to ZnTPP increases the driving force for charge separation while it decreases the driving force for charge recombination. This is in line with the lifetimes observed experimentally, explaining the stronger inhibiting effect being for the charge recombination rather than for the charge separation.

In contrast to the supramolecular system, the control TRIR experiment with 2.0 mM [μ-($PhCH_2$−NMI-S_2)$Fe_2(CO)_6$] (**3a**) (the pyridyl-lacking analogue of **3**, Chart 1) and 2.0 mM ZnTPP under identical conditions revealed no electron transfer (Supporting Information, Figure S12). All these results indicate that the photoinduced electron transfer requires the formation of the self-assembly between the pyridyl-N and the porphyrin zinc center. To confirm this, we performed control TRIR experiment with 2.0 mM **3** in the absence of ZnTPP, in which we observed an ultrafast spectral change within 1 ps, which decayed within *ca.* 200 ps while the maximum intensity of the transient signal reached only *ca.* 5% compared to that obtained for the **3**·ZnTPP assembly (see Supporting Information, Figure S13 for a direct comparison). These small transient signals are not associated with the one-electron reduction of **3**, but with CO dissociation and reorganization of the FeFe bond.[17,18]

Notably, the ν(C≡O) frequencies of the carbonyls at the diiron center shifted in average by *ca.* 27 cm^{-1} to lower energy upon the one-electron transfer from the photoexcited porphyrin to complex **3**. At the same time, the $\nu(C{=}O)_{NMI}$ frequencies of the monoimide group shifted from 1705 and 1668 to 1628 cm^{-1}, as shown in Figure 3b, in line with the dominant photoreduction of the monoimide. The IR wavenumber changes obtained with TRIR provide an important information for analyzing the electronic structure of the reduced species.

In the ground state, the reduction of several diiron dithiolate complexes was studied previously by IR spectroelectrochemistry (IR SEC) to characterize the unstable one-electron reduced core, Fe^0Fe^I.[3b,15b,19] For a direct comparison with the TRIR spectra obtained above, we carried out the electrochemical reduction of complex **3** in CH_2Cl_2 within an OTTLE cell.

The IR spectrum of stable electro-generated $\mathbf{3}^{\bullet-}$ (Figure 3c,d) matched well that of the photoproduct encountered in the TRIR experiments, directly confirming that the one-electron transfer from photoexcited ZnTPP to complex **3** took place during the TRIR measurement. Upon electrochemical reduction, the carbonyl stretching frequencies of the diiron core and imide group both shifted to lower energy, by 28 cm^{-1} for ν(C≡O) and 80 cm^{-1} for $\nu(C{=}O)_{NMI}$ (the second band accompanying that at 1629 cm^{-1} was observed at 1583 cm^{-1} for $\mathbf{3}^{\bullet-}$, see Supporting Information, Figure S14), respectively. Importantly, the red shift ($\Delta\nu_{av}$(C≡O) = 28 cm^{-1}) of the carbonyls on iron was much smaller compared to values reported for the one-electron reduction $Fe^IFe^I \rightarrow Fe^0Fe^I$ in hexacarbonyl complexes, for example, [(μ-$S_2C_3H_6$)$Fe_2(CO)_6$] ($\Delta\nu_{av}$(C≡O) ≈ 70 cm^{-1}),[15b] [(μ-SEt)$_2$$Fe_2(CO)_6$] ($\Delta\nu_{av}$(C≡O) ≈ 76 cm^{-1})[3b] and [(μ-bpdt)$Fe_2(CO)_6$] (bpdt = biphenyl-2,2′-dithiolate, $\Delta\nu_{av}$(C≡O) ≈ 80 cm^{-1}).[19] The reported 70−80 cm^{-1} red shift corresponds to the one-electron reduction of FeFe core, strongly suggesting the dominant reduction of the NMI group over the diiron center in complex **3** during both photoinduced and electrochemical one-electron reduction. The electron density at the π-conjugated NMI bridge in $\mathbf{3}^{\bullet-}$ is in line with the DFT-calculated spin density plot shown in Figure 4. A comparable localization of spin density on the non-innocent quinone bridge in [(μ-$S_2C_{10}H_4O_2$)-$Fe_2(CO)_4(PPh_3)_2$]$^{\bullet-}$ was recently reported by Glass and co-workers[20] during the preparation of this manuscript. In a previous report, very small spin density delocalization over the diiron core ($\Delta\nu_{av}$(C≡O) ≈ 5 cm^{-1}) was observed for the one-electron-reduced [(μ-bdt)$Fe_2(CO)_5(C_{60}(H)PPh_2)$]$^{\bullet-}$ bearing a fullerene-functionalized ligand.[21] The spin density localized in the diiron orbital in $\mathbf{3}^{\bullet-}$ was calculated as 0.23 e^{-1}. In the DFT-optimized $\mathbf{3}^{\bullet-}$, the Fe−Fe distance is 2.557 Å, that is *ca.* 0.05 Å longer than that of **3** in the solid state, in line with the electron density distributed over the diiron center.

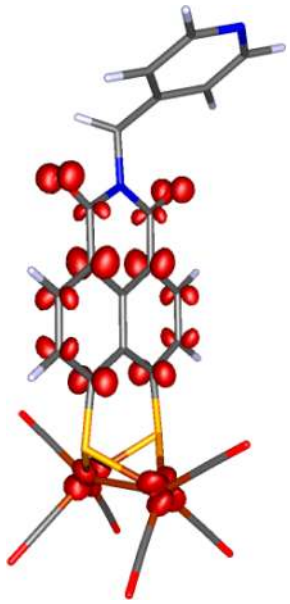

Figure 4. Spin density plot (BP86, def2-TZVP) for [μ-(4-pyCH_2−NMI-S_2)$Fe_2(CO)_6$]$^{\bullet-}$ ($\mathbf{3}^{\bullet-}$).

IR Spectroelectrochemical and DFT Study of Compound 1. As a reference complex bearing a naphthalene ring without monoimide group, [(μ-naphdt)$Fe_2(CO)_6$] (naphdt = naphthalene-1,8-dithiolate, **1**),[14] was used for the IR SEC monitoring of the reduction under identical conditions (Figure 5, top). The ν(C≡O) red shift ($\Delta\nu_{av}$(C≡O) ≈ 79 cm^{-1}) observed for the reduction of **1** to $\mathbf{1}^{\bullet-}$ closely resembles the reported examples outlined above, being indeed much larger than that observed for complex **3**, where the acceptor NMI group strongly determines the cathodic path. In the DFT-optimized $\mathbf{1}^{\bullet-}$, the Fe−Fe bond is considerably weakened and the distance reduced to 2.81 Å, which is 0.3 Å longer compared to **1** in the solid state.[14] The spin density localized on the diiron center is 0.75 e^{-1} (Figure 5, bottom), being equally distributed over two iron atoms. The dominant reduction of the Fe−Fe bond in **1**, which is different from the actual reduction of an Fe−S bond in [(μ-bpdt)$Fe_2(CO)_6$] (bpdt = biphenyl-2,2′-dithiolate),[19] was further supported by EPR spectroscopy and theoretical calculations discussed below in the EPR spectroscopy section.

The spin density at the Fe_2 centers in $\mathbf{1}^{\bullet-}$ and $\mathbf{3}^{\bullet-}$ exhibits a nice correlation with the IR ν(C≡O) shifts, in agreement with the reduction of different moieties (the different lowest unoccupied molecular orbitals characters) revealed by the theoretical calculations. Figure 6 shows the accurate linear correlation between the experimentally measured average low-energy IR shifts of the terminal carbonyls, $\Delta\nu_{av}$(C≡O), reflecting the one-electron reduction, and the theoretically calculated spin density on the Fe_2 core; the data for **3**-dppv

dx.doi.org/10.1021/ic500777d | *Inorg. Chem.* 2014, 53, 5373−5383

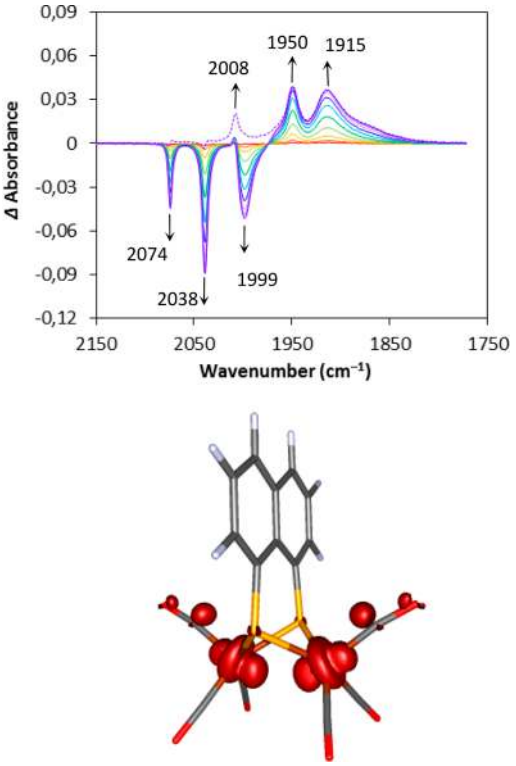

Figure 5. (top) Absorbance difference IR SEC spectra recorded during the one-electron reduction of 1.0 mM [(μ-naphdt)$Fe_2(CO)_6$] (**1**) in CH_2Cl_2 (0.1 M nBu_4NPF_6) within an OTTLE cell at 293 K. The dashed purple line was extracted to show the IR absorption of $\mathbf{1}^{\bullet-}$, whereof especially the ν(C≡O) band at 2008 cm^{-1} that was largely hidden in the resulting difference spectra. (bottom) Spin density plot (BP86, def2-TZVP) for [(μ-naphdt)$Fe_2(CO)_6$]$^{\bullet-}$ ($\mathbf{1}^{\bullet-}$).

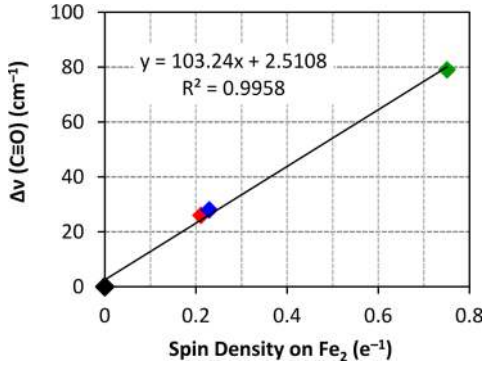

Figure 6. Linear correlation between $\Delta\nu$(C≡O) and the spin density population at the Fe_2 core. Values for IR shifts were determined from the IR SEC monitoring of the reduction of [(μ-naphdt)$Fe_2(CO)_6$] (**1**, green), [μ-(4-pyCH_2–NMI-S_2)$Fe_2(CO)_6$] (**3**, blue), and [μ-(4-pyCH_2–NMI-S_2)$Fe_2(CO)_4$(dppv)] (**3**-dppv, red).

(Supporting Information, Figure S15) and zero point were included in the linear fitting. The ν(C≡O) values serve as a convenient quantitative probe to evaluate the degree of the reduction/spin density localization on the Fe_2 center in these diiron hexacarbonyl complexes. The full set of DFT-calculated data for the frontier orbitals and spin density plots for complexes **1**, **3**, and **3**-dppv can be found in the Supporting Information (Figures S16–18).

EPR Spectroscopy. In toluene at 293 K, mixing of [μ-(4-pyCH_2–NMI-S_2)$Fe_2(CO)_6$] (**3**) ($E_{1/2}$ = −1.28 V vs Fc/Fc^+) and 1 equiv of Cp_2Co (Cp = cyclopentadienyl) ($E_{1/2}$ = −1.33 V vs Fc/Fc^+)[22] gave no redox reaction as revealed by IR spectroscopy (temperature- and solvent-dependent reduction of **3** by Cp_2Co was observed, see Figures S19–22 and corresponding discussion in the Supporting Information), and the yellow color of parent **3** was maintained. In contrast, the solution color turned deep blue immediately after the addition of 1 equiv of Cp^*_2Co ($E_{1/2}$ = −1.94 V vs Fc/Fc^+)[22] to **3**; IR spectroscopy at the same time confirmed the formation of $\mathbf{3}^{\bullet-}$. In addition, strong absorption at 602 and 790 nm was observed for $\mathbf{3}^{\bullet-}$ by UV–vis SEC experiment (Supporting Information, Figure S20), in agreement with the color turning blue. The freshly prepared blue solution of $\mathbf{3}^{\bullet-}$ was used for EPR spectroscopic measurement at RT. As shown in Figure 7 (top)

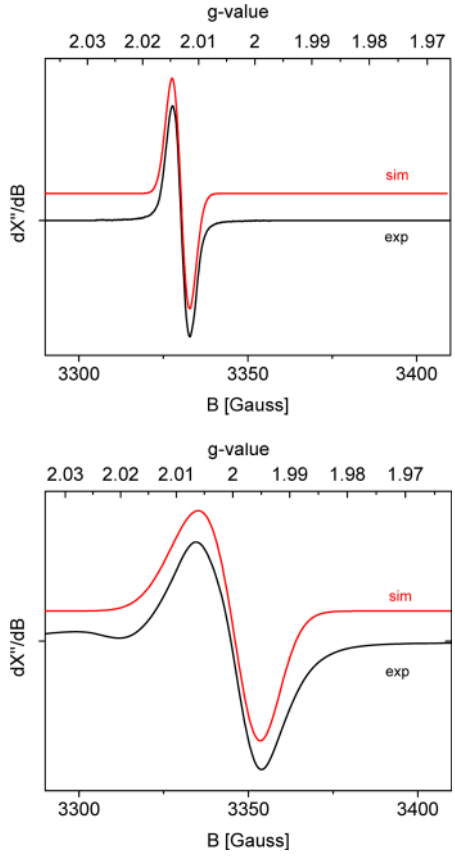

Figure 7. (top) Experimental and simulated X-band EPR spectrum of [μ-(4-pyCH_2–NMI-S_2)$Fe_2(CO)_6$]$^{\bullet-}$ ($\mathbf{3}^{\bullet-}$). Experimental conditions: T = 293 K, microwave power of 0.2 mW, field modulation amplitude of 0.1 G, modulation frequency of 9.383 319 GHz. The sample was prepared by chemical reduction of **3** with 1 equiv of Cp^*_2Co in toluene at 293 K in a glovebox. (bottom) Experimental and simulated X-band EPR spectrum of [(μ-naphdt)$Fe_2(CO)_6$]$^{\bullet-}$ ($\mathbf{1}^{\bullet-}$). Experimental conditions: T = 10 K, microwave power of 2.0 mW, field modulation amplitude of 4 G, modulation frequency of 9.364 522 GHz. The sample was prepared by chemical reduction of **1** with 1 equiv of Cp^*_2Co in dichloromethane at 195 K under Ar.

a well-defined, relatively sharp isotropic EPR signal lacking a hyperfine structure was detected at 293 K. The signal reveals an isotropic g-value of 2.013, in a good agreement with the DFT-calculated g_{iso} value of 2.012. This is in line with the DFT-calculated electronic structure showing that the unpaired electron of $\mathbf{3}^{\bullet-}$ mainly located in an NMI-centered orbital.

dx.doi.org/10.1021/ic500777d | Inorg. Chem. 2014, 53, 5373–5383

Table 1. IR Spectroscopic Data for 1, 3,3a, 3-dppv and Their Radical Anions

compound[a]	ν(C≡O)	$\Delta\nu_{av}$(C≡O)[b]	ν(C═O)$_{NMI}$	$\Delta\nu_{av}$(C═O)$_{NMI}$[b]
[(μ-naphdt)Fe$_2$(CO)$_6$] (**1**)	2074, 2038, 1999			
[(μ-naphdt)Fe$_2$(CO)$_6$]$^{\bullet-}$ (**1**$^{\bullet-}$)	2008, 1950, 1915	79		
[μ-(4-pyCH$_2$–NMI-S$_2$)Fe$_2$(CO)$_6$] (**3**)	2080, 2046, 2007		1706, 1666	
[μ-(4-pyCH$_2$–NMI-S$_2$)Fe$_2$(CO)$_6$]$^{\bullet-}$ (**3**$^{\bullet-}$)	2054, 2018, 1976	28	1629, 1583	80
[μ-(PhCH$_2$–NMI-S$_2$)Fe$_2$(CO)$_6$] (**3a**)	2079, 2045, 2006		1703, 1663	
[μ-(PhCH$_2$–NMI-S$_2$)Fe$_2$(CO)$_6$]$^{\bullet-}$ (**3a**$^{\bullet-}$)	2051, 2016, 1977	28	1627, 1582	79
[μ-(4-pyCH$_2$–NMI-S$_2$)Fe$_2$(CO)$_4$(dppv)] (**3**-dppv)	2031, 1964, 1920		1699, 1659	
[μ-(4-pyCH$_2$–NMI-S$_2$)Fe$_2$(CO)$_4$(dppv)]$^{\bullet-}$ [(**3**-dppv)$^{\bullet-}$]	2005, 1934, 1898	26	1616, 1573	84

[a]Experiments were conducted in CH_2Cl_2, data for radical anions were extracted from IR SEC. [b]The average IR bands shift during the one-electron reduction of the corresponding neutral compound.

Attempts to record an isotropic EPR spectrum of [(μ-naphdt)Fe$_2$(CO)$_6$]$^{\bullet-}$ (**1**$^{\bullet-}$) in solution were not successful. At 10 K, a rather broad near isotropic signal was detected at g = 2.0045, together with a weak signal ($g \approx 2.027$) stemming from an unknown impurity (Figure 7, bottom). The signal of **1**$^{\bullet-}$ is much broader than that of **3**$^{\bullet-}$, and spectral simulation points to a small rhombicity of the g-tensor (g_{11} = 2.0066, g_{22} = 2.0045, g_{33} = 2.0000; g_{av} = 2.0045). The DFT-calculated g-tensor (g_{11} = 2.0066, g_{22} = 2.0045, g_{33} = 2.0017; g_{av} = 2.0043) corresponds quite well with the measurement, giving support to the electronic structure presented in Figure 5, showing that the unpaired electron is mainly located at the diiron center of the mixed-valent Fe^0Fe^I system.

Photoinduced H_2 Production. TRIR spectroscopy documented the photoinduced electron transfer from ZnTPP to complex **3**, which can be the first step in the catalytic cycle of H_2 formation. Photogeneration of molecular hydrogen was attempted by irradiating complex **3** (4 μmol) with a 500 W Xe lamp ($\lambda \leq$ 530 nm was removed by a cutoff filter to prevent direct photoexcitation and consequent degradation of the Fe_2S_2 complex) in the presence of the light harvesting chromophore (ZnTPP, 4 μmol), a proton source (HOAc, 22 μmol) and a bulky sacrificial electron donor (^{i}Pr$_2$NEt, 22 μmol) in toluene (5 mL). Only a very small amount (*ca.* 5 μL) of dihydrogen was detected by an online gas chromatograph system (Supporting Information, Figure S23). The formation of molecular hydrogen was likely due to a noncatalytic photolysis process. The spin density in **3**$^{\bullet-}$ largely delocalized over the NMI group after the electron transfer to the Fe_2S_2 complex, prevented the following reaction with protons. This behavior is consistent with the noncatalytic nature of the cathodic cyclic voltammogram of **3** recorded in the presence of acetic acid (Supporting Information, Figure S24).

CO Substitution with dppv in 3. In an attempt to make the Fe_2S_2 complexes more reactive toward protonation, a CO substitution reaction was carried out to make the iron centers more electron rich. Complex [μ-(4-pyCH$_2$–NMI-S$_2$)-Fe$_2$(CO)$_4$(dppv)] (**3**-dppv, dppv = *cis*-1,2-bis-(diphenylphosphino)ethylene) was readily obtained (86% yield) by the reaction of complex **3** with 1 equiv of dppv in CH_2Cl_2 at RT. Complex **3**-dppv displays three ν(C≡O) bands at 2030, 1962, 1920 cm^{-1}, and two ν(C═O)$_{NMI}$ bands at 1697 and 1658 cm^{-1} (Supporting Information, Figure S15 and Table 1). The substitution of two carbonyl ligands with chelating dppv leads to an average shift of ν(C≡O) bands by 73 cm^{-1} to lower energy, which is comparable with the literature data reported for [(μ-pdt)Fe$_2$(CO)$_4$(dppv)] and [(μ-edt)-Fe$_2$(CO)$_4$(dppv)] by Rauchfuss and co-workers.[23] Table 1 summarized the IR data for the compounds related to this study.

Single-crystal X-ray diffraction (Figure 8, left) reveals that the Fe–Fe bond in **3**-dppv is significantly lengthened to 2.5510(5)

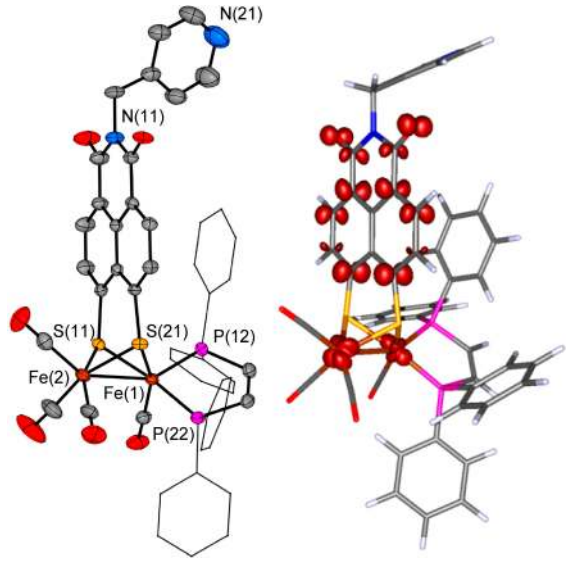

Figure 8. (left) Molecular structure of [μ-(4-pyCH$_2$–NMI-S$_2$)-Fe$_2$(CO)$_4$(dppv)] (**3**-dppv) in the crystal with displacement ellipsoids drawn at the 50% probability level. Disordered CH_2Cl_2 solvent molecules, hydrogen atoms and phenyl ellipsoids on dppv have been omitted for clarity. Selected bond lengths (Å) and angles (deg): Fe(1)–Fe(2), 2.5510(5); Fe(1)–S(11), 2.2331(6); Fe(1)–S(21), 2.2270(5); Fe(2)–S(11), 2.2631(6); Fe(2)–S(21), 2.2594(6); Fe(2)–CO$_{ap}$, 1.795(3); Fe(2)–CO$_{ba}$, 1.782(3); Fe(1)–P(12), 2.1767(6); Fe(1)–P(22), 2.2159(6); Fe(1)–CO$_{ba}$, 1.754(2); S(21)–Fe(2)–S(11), 83.68(2); S(21)–Fe(1)–S(11), 85.12(2); S(11)–Fe(2)–Fe(1)–S(21), 109.40(3). (right) Spin density plot (BP86, def2-TZVP) for (**3**-dppv)$^{\bullet-}$.

Å from 2.50955(16) Å in **3** due to the electron donating ligand, dppv, indicating the electron rich character of the Fe–Fe bond in **3**-dppv (see Supporting Information, Figure S18 for the frontier orbitals). As a result, the average Fe–CO$_{ba}$ bond was shortened from 1.8057(9) and 1.8024(8) in 3 to 1.754(2) Å in **3**-dppv by the enhanced π back-donating effect. The rotation of the chelating dppv ligand in solution was proven by variable temperature (VT)-NMR measurements (Supporting Information, Figure S25). As shown in Figure 8 (right), the dppv substitution imposed slight changes in the spin density distribution in (**3**-dppv)$^{\bullet-}$ (0.21 e^{-1} on Fe_2), which is further supported by the IR SEC result ($\Delta\nu$(C≡O) = 26 cm^{-1}, shown

dx.doi.org/10.1021/ic500777d | *Inorg. Chem.* 2014, 53, 5373–5383

in Supporting Information, Figure S15). The correlation between spin density distribution and IR shift for (**3**-dppv)$^{\bullet-}$ was incorporated in the linear fitting shown in Figure 6.

A steady state fluorescence titration of ZnTPP with complex **3**-dppv revealed the formation of self-assembled **3**-dppv·ZnTPP with an association constant as K_{ass} = 5.5 × 10^3 mol^{-1} dm^3 (Supporting Information, Figure S26), which is comparable to that for **3**·ZnTPP. The Stern−Volmer quenching constant was calculated to be K_{SV} = 1.6 × 10^4 mol^{-1} dm^3, strongly suggesting that the ZnTPP was quenched by the electron transfer to **3**-dppv (Supporting Information, Figure S27).

The first reduction potential of **3**-dppv was found at −1.48 V, that is, negatively shifted by *ca.* 200 mV compared to that for parent complex **3** (Table 2). The potential shift caused by the dppv ligation is smaller than that expected for a chelating diphosphine ligand, while comparable to that resulted from the CO-to-PPh_3 monosubstitution (the first reduction potential negatively shifted by 210 mV) in [(μ-pdt)$Fe_2(CO)_6$].[24] The spin density in (**3**-dppv)$^{\bullet-}$, again mainly distributed over the NMI group, explains the decreased effect of the dppv/CO substitution on the redox potentials. Cyclic voltammetry in the presence of HOAc showed no catalytic proton reduction activity for **3**-dppv around its first reduction wave (−1.48 V) (Supporting Information, Figure S28). A slightly larger amount of H_2 (20 μL, turnover number (TON) ≈ 0.2) was detected in the presence of **3**-dppv (Supporting Information, Figure S23), which proved to be more stable than **3** on irradiation under the same conditions. The activity (up to 0.2 TON) achieved by this assembly is significantly lower compared to the previously reported efficient photodriven H_2 evolution systems based on earth-abundant metal catalysts.[4,25]

The EPR spectrum of (**3**-dppv)$^{\bullet-}$, generated from **3**-dppv via one-electron reduction with 1 equiv of Cp*Co in toluene solution as 293 K, reveals an isotropic signal with a *g*-value of 2.0140. Hyperfine couplings are partially resolved. Simulation of the spectrum was possible after inspection of the DFT-calculated EPR parameters. The spectrum is dominated by the hyperfine coupling with two sets of equivalent protons from the NMI moiety (H1 and H2) and two nonequivalent phosphorus nuclei (P1 and P2; labeling shown in Figure 9). A satisfactory simulation was obtained using similar hyperfine couplings as in the DFT calculations, although it was necessary to make the proton hyperfine coupling significantly larger to obtain a good fit (see Figure 9 and Table 3).

Table 2. Cathodic Potentials of 3, 3a, and 3-dppv

compound	$E_{1/2}^1$ (V), (ΔE_p (mV))[a]	$E_{1/2}^2$ (V), (ΔE_p (mV))[a]
[(μ-naphdt)$Fe_2(CO)_6$] (**1**)[b]	−1.67, (−)	−2.00, (−)
[μ-(4-pyCH_2−NMI-S_2)$Fe_2(CO)_6$] (**3**)	−1.28, (92)	−1.65, (84)
[μ-(PhCH_2−NMI-S_2)$Fe_2(CO)_6$] (**3a**)	−1.29, (93)	−1.65, (102)
[μ-(4-pyCH_2−NMI-S_2) $Fe_2(CO)_4$(dppv)] (**3**-dppv)	−1.48, (88)	−2.02[c]

[a]All potentials are reported vs Fc/Fc^+ used as an internal standard. [b]Reference 14. [c]E_{pc} for irreversible reduction.

CONCLUSIONS

TRIR spectroscopic study of complex **3** was successfully conducted to characterize for the first time an ultrafast electron transfer process between excited ZnTPP and a Fe_2S_2 H_2-ase model in a self-assembled system. The lifetimes of the charge separation (CS) and charge recombination (CR) processes were calculated from curve fitting as τ_{CS} = 40 ± 3 ps and τ_{CR} = 205 ± 14 ps, respectively. Compared to the covalently bound model **2**-ZnP, both processes but especially the charge recombination were dramatically slowed down in the supramolecular assembly **3**·ZnTPP, as a result of the difference in relative orientation of the photosensitizer with respect to the electron acceptor and the coordination of a pyridyl group to the Zn(TPP). The electronic structure of reduced **3**$^{\bullet-}$ was studied by IR spectroelectrochemistry (IR SEC), EPR spectroscopy, and DFT calculations. The combined results reveal that the NMI group is noninnocent during the first reduction of complex **3**, which explains the low activity in photodriven hydrogen production. The current results suggest a clear outlook for future directions in this research. New complexes should be prepared with redox innocent bridges that tune the reduction potentials of Fe_2S_2 mimics properly while avoiding delocalization of the spin density. Such systems are anticipated to lead to active bioinspired Fe_2S_2 catalysts for photodriven hydrogen evolution. This study shows that TRIR is a powerful tool for the characterization of the ultrafast electron transfer process between the photoexcited chromophore and the Fe_2S_2 hydrogenase model.

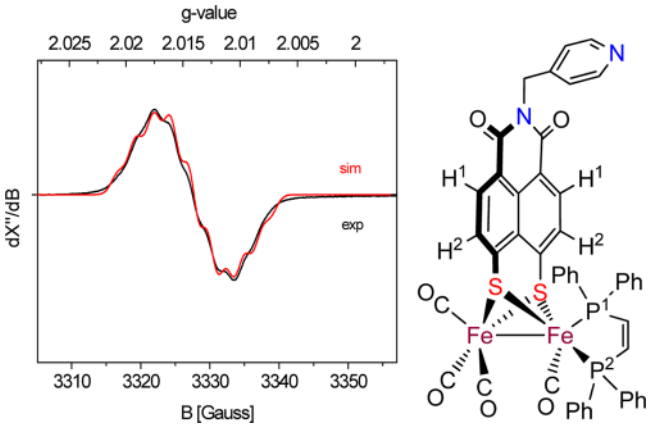

Figure 9. Experimental and simulated X-band EPR spectrum of [μ-(4-pyCH_2−NMI-S_2)$Fe_2(CO)_4$(dppv)]$^{\bullet-}$ [(**3**-dppv)$^{\bullet-}$]. Experimental conditions: *T* = 293 K, microwave power of 0.2 mW, field modulation amplitude of 0.1 G, modulation frequency of 9.380 295 GHz. The sample was prepared by chemical reduction of **3** with 1 equiv of Cp*$_2$Co in toluene at RT in a glovebox.

Table 3. Experimental and DFT-Calculated EPR Parameters of (3-dppv)$^{\bullet-}$

	exp.[a]	DFT[b]
g-value	2.0140	2.0121
A^{H1}_{iso}[c]	13.5[c]	7.3[c]
A^{H2}_{iso}[c]	6.5[c]	1.6[c]
A^{P1}_{iso}	6.0	4.7
A^{P2}_{iso}	9.5	9.6

[a]On the basis of spectral simulation; see Figure 9. [b]Orca, B3LYP, def2-TZVP. [c]Two equivalent protons.

EXPERIMENTAL SECTION

General Procedures. All manipulations were performed under a nitrogen or argon atmosphere, using standard Schlenk techniques, or in a glovebox. Commercially available chemicals,

dx.doi.org/10.1021/ic500777d | Inorg. Chem. 2014, 53, 5373−5383

4-(aminomethyl)pyridine, $Fe_2(CO)_9$, and *cis*-1,2-bis-(diphenylphosphino)ethene were used as received from Aldrich. The supporting electrolyte nBu$_4$NPF$_6$ was recrystallized from methanol and dried under vacuum at 80 °C overnight. 1,8-Naphthalic anhydride-4,5-disulfide[26] and [(μ-naphdt)$Fe_2(CO)_6$] (**1**, naphdt = naphthalene-1,8-dithiolate)[14] were synthesized by literature procedures. The ^{1}H, ^{13}C, and ^{31}P NMR spectra were collected with a Bruker AVANCE 400 spectrometer. IR spectra were recorded with a Nicolet Nexus FT-IR spectrometer. Elemental analyses were performed with a PerkinElmer 2400 elemental analyzer. HR-MS were obtained on a time-of-flight JEOL AccuTOF LC-plus mass spectrometer (JMS-T100LP).

*[4-pyCH$_2$–NMI-S$_2$] (**L**).* 4-(Aminomethyl)pyridine (2.7 g, 25 mmol) was added to a suspension of 1,8-naphthalic anhydride-4,5-disulfide (1.1 g, 4.2 mmol) in 2-methoxyethanol (60 mL) at RT. The mixture was refluxed for 48 h under N_2. After the mixture cooled to RT, golden plate crystals that formed rapidly were collected by filtration, washed with diethyl ether (3× 20 mL), and dried under vacuum. Yield: 0.8 g (54%). Crystals suitable for X-ray diffraction were obtained by recrystallization in hot chlorobenzene. ^{1}H NMR (400 MHz, $CDCl_3$): δ 8.52 (d, $^3J_{HH}$ = 6.1 Hz, 2H, Py), 8.45 (d, $^3J_{HH}$ = 8.1 Hz, 2H, Naph), 7.51 (d, $^3J_{HH}$ = 8.1 Hz, 2H, Naph), 7.34 (d, $^3J_{HH}$ = 6.0 Hz, 2H, Py), 5.36 (s, 2H, CH_2) ppm. ^{13}C NMR (101 MHz, $CDCl_3$): δ 163.26, 154.14, 148.14, 134.17, 133.56, 130.67, 124.00, 116.95, 116.72, 42.83 ppm. IR (CH_2Cl_2, cm^{-1}): ν(C═O)$_{NMI}$ 1692 (w), 1655 (w). HR-MS time-of-flight electrospray ionization (TOF-ESI+) Calcd for $C_{18}H_{11}N_2O_2S_2$ [M + H]$^+$: 351.0262; found 351.262. Anal. Calcd for $C_{18}H_{10}N_2O_2S_2$: C 61.70, H 2.88, N 7.99; found: C 61.34, H 3.07, N 8.00%.

*[PhCH$_2$–NMI-S$_2$] (**La**).* A similar procedure for the synthesis of **L** was applied by using benzylamine instead of 4-(aminomethyl)pyridine. Yield: 0.8 g (66%). ^{1}H NMR (400 MHz, DMSO-d_6): δ 8.33 (d, $^3J_{HH}$ = 8.1 Hz, 2H, Naph), 7.85 (d, $^3J_{HH}$ = 8.1 Hz, 2H, Naph), 7.38–7.16 (m, 5H, Ph), 5.24 (s, 2H, CH_2) ppm. ^{13}C NMR (101 MHz, $CDCl_3$): δ 163.40, 153.32, 137.64, 134.01, 133.25, 129.88, 129.03, 128.55, 127.53, 117.34, 116.77, 43.71 ppm. IR (CH_2Cl_2, cm^{-1}): ν(C═O)$_{NMI}$ 1690 (w), 1653 (w). Anal. Calcd for $C_{19}H_{11}NO_2S_2$: C 65.31, H 3.17, N 4.01; found: C 65.02, H 3.02, N 4.00%.

*[μ-(4-pyCH$_2$–NMI-S$_2$)Fe$_2$(CO)$_6$] (**3**).* THF (50 mL) was added to a mixture of **L** (100 mg, 0.28 mmol) and $Fe_2(CO)_9$ (208 mg, 0.57 mmol) under N_2 at RT. After it was stirred for 1 h at RT, the mixture was filtered through Celite. The solution was collected and dried by vacuum. The resulting dark solid was purified by column chromatography on Silica gel (60–200 μm) with CH_2Cl_2 and MeOH (100:0.3, v/v) as eluent. The analytically pure solid of **3** was obtained as an orange powder. Yield: 90 mg (50%). Crystals suitable for X-ray diffraction were collected by diffusion of pentane into the CH_2Cl_2 solution of 4 at −20 °C. ^{1}H NMR (400 MHz, acetone-d_6) δ 8.67 (d, $^3J_{HH}$ = 6.7 Hz, 2H, Py), 8.63 (d, $^3J_{HH}$ = 7.7 Hz, 2H, Naph), 8.44 (d, $^3J_{HH}$ = 7.7 Hz, 2H, Naph), 7.54 (d, $^3J_{HH}$ = 6.7 Hz, 2H, Py), 5.37 (s, 2H, CH_2) ppm. ^{13}C NMR (101 MHz, acetone-d_6) δ 208.06, 163.91, 158.39, 150.67, 149.76, 135.27, 134.22, 130.44, 126.49, 126.15, 125.83, 43.14 ppm. IR (CH_2Cl_2, cm^{-1}): ν(C≡O) 2080 (s), 2046 (s), 2007 (s); ν(C═O)$_{NMI}$ 1706 (w), 1666 (w). HR-MS (TOF-ESI+) Calcd for $C_{24}H_{11}Fe_2N_2O_8S_2$ [M + H]$^+$: 630.8657; found 630.8638%.

*[μ-(PhCH$_2$–NMI-S$_2$)Fe$_2$(CO)$_6$] (**3a**).* THF (50 mL) was added to a mixture of **La** (100 mg, 0.28 mmol) and $Fe_2(CO)_9$ (208 mg, 0.57 mmol) under N_2 at RT. After it was stirred for 1 h at RT, the mixture was filtered through Celite. The solution was collected and dried by vacuum. The resulting dark solid was purified by column chromatography on Silica gel (60–200 μm) with CH_2Cl_2 and hexane (3:2, v/v) as eluent. The analytically pure solid of **3a** was obtained as an orange powder. Yield: 115 mg (64%). ^{1}H NMR (400 MHz, acetone-d_6): δ 8.62 (d, 2H, $^3J_{HH}$ = 7.7 Hz, Naph), 8.45 (d, 2H, $^3J_{HH}$ = 7.7 Hz, Naph), 7.46 (d, 2H, $^3J_{HH}$ = 7.5 Hz, Ph), 7.31–7.21 (m, 3H, Ph) ppm. ^{13}C NMR (101 MHz, acetone-d_6): δ 208.09, 163.79, 138.34, 134.90, 134.20, 130.37, 130.15, 129.15, 129.12, 128.06, 126.45, 126.30, 44.18 ppm. IR (CH_2Cl_2, cm^{-1}): ν(C≡O) 2079 (s), 2045 (s), 2006 (s); ν(C═O)$_{NMI}$ 1703 (w), 1663 (w). Anal. Calcd for $C_{25}H_{11}Fe_2NO_8S_2$: C 47.72, H 1.76, N 2.23; found: C 47.67, H 1.47, N 2.19%.

[μ-(4-pyCH$_2$–NMI-S$_2$)Fe$_2$(CO)$_4$(dppv)] (3-dppv). To a solution of **3** (90 mg, 0.14 mmol) in CH_2Cl_2 (10 mL) was added *cis*-1,2-bis(diphenylphosphino)ethene (dppv) (60 mg, 0.15 mmol) in CH_2Cl_2 (5 mL). The mixture was stirred for 12 h at RT. The resulting greenish brown solution was concentrated to *ca.* 1 mL, and then hexane (10 mL) was added to precipitate the crude product as light brown powders. Yield: 120 mg (86%). Crystals suitable for X-ray diffraction were obtained by diffusion of pentane into the CH_2Cl_2 solution of **3**-dppv. ^{1}H NMR (400 MHz, $CDCl_3$): δ 8.70 (d, 2H, $^3J_{HH}$ = 6.5 Hz, Naph), 8.52 (s, 2H, Py), 8.2–7.5 (m, 20H, Ph), 7.46 (d, 2H, $^3J_{HH}$ = 6.3 Hz, Naph), 5.32 (s, 2H, CH_2), 5.27 (s, 2H, PCH) ppm. ^{13}C NMR (101 MHz, acetone-d_6): δ 164.01, 150.73, 147.36, 134.39, 134.29, 132.31, 131.89, 131.77, 131.64, 129.84, 129.71, 129.62, 128.51, 128.43, 123.72, 123.30, 43.02 ppm. ^{31}P NMR (162 MHz, acetone-d_6): δ 96.76 ppm. IR (CH_2Cl_2, cm^{-1}): ν(C≡O) 2031(s), 1965 (s), 1923 (w); ν(C═O)$_{NMI}$ = 1699 (w), 1659 (w). HR-MS (TOF-atomospheric pressure chemical ionization (APCI)+) Calcd for $C_{48}H_{33}Fe_2N_2O_6P_2S_2$ [M + H]$^+$: 970.9956; found 970.9924. Anal. Calcd for $C_{48}H_{32}Fe_2N_2O_6P_2S_2\cdot 0.5CH_2Cl_2$: C 57.50, H 3.28, N 2.77; found: C 57.31, H 3.03, N 2.77%.

Spectroelectrochemistry. Cyclic voltammograms were recorded using an Autolab PGSTAT302N electrochemical workstation, and an airtight three-electrode cell under dry N_2. The working electrode was a carefully polished Pt microdisc (diameter 0.5 mm). A coiled Pt wire was used as a counter electrode and a coiled Ag wire as the pseudoreference electrode. All electrode potentials reported in this work are referenced versus the internal standard ferrocene/ferrocenium (Fc/Fc$^+$) couple.[21] The measurements were performed on 1.0 mM complexes in CH_2Cl_2 containing 0.1 M nBu$_4$NPF$_6$ as a supporting electrolyte. Cyclic voltammograms in the presence of HOAc were recorded using the same setup while a polished glassy carbon disc (diameter 3 mm) was used as a working electrode. IR SEC was performed in an optically transparent thin-layer (200 μm) electrochemical (OTTLE) cell[27] equipped with CaF_2 optical windows and a platinum minigrid working electrode. The difference absorbance IR spectra were recorded on a Nicolet Nexus FT-IR spectrometer in the course the thin-layer cyclic voltammetry scanning process (ν = 2 mV s^{-1} controlled by a PGSTAT 10 (Eco-Chemie) potentiostat (see Supporting Information, Figure S9 for a thin-layer cyclic voltammetry response).

Steady-State UV–vis Absorption and Emission. UV–vis absorption spectra in the titration experiments were measured on a Shimadzu UV-2700 spectrophotometer, using 2 mm quartz cuvettes. Emission spectra were measured on a Spex Fluorolog 3 spectrofluorimeter, equipped with double

dx.doi.org/10.1021/ic500777d | Inorg. Chem. 2014, 53, 5373–5383

grating monochromators in the excitation and emission channels. The excitation light source was a 450W Xe lamp and the detector a Peltier cooling R636−10 (Hamamatsu) photomultiplier tube. The CH_2Cl_2 solution of the ligand or complexes **3**, **3**-dppv (1.6×10^{-3} M) were prepared by dissolving the corresponding compound in the ZnTPP solution (8.0×10^{-5} M) to keep the concentration of ZnTPP constant during the titration experiment.

Time-Resolved Infrared Spectroscopy. Tunable visible pump and mid-IR probe were generated using a Ti:sappahire laser (Spectra-Physics Hurricane, 600 μJ) with a repetition rate of 1 kHz pumping two commercial BBO-based OPAs (Spectra-Physics OPA-800C). Visible pump pulses (553 nm) were generated by sum-frequency mixing the Ti:sapphire pump and idler (centered at 1791 nm) of one of the OPAs in BBO (UV pulse energy = 3 μJ); IR probe pulses were generated by difference-frequency mixing signal and idler from the other OPA in $AgGaS_2$, for details see ref 28. The sample cell with CaF_2 windows spaced by 500 μm was replaced in the IR focus. Using a Newport ESP300 translation stage, the delay positions were scanned by mechanically adjusting the beam-path of the UV pump. The temporal resolution of 200 fs has been obtained from full width at half-maximum of the pump probe cross-correlate function. The transient spectra were obtained by subtracting nonpumped absorption spectra from the pumped absorption spectra that were recorded by a custom built 30 pixel MCT detector coupled to an Oriel MS260i spectrograph.

EPR Spectroscopy and Simulation. Experimental X-band EPR were recorded on a Bruker EMX plus spectrometer equipped with a He temperature control cryostat system (Oxford Instruments). The spectra were simulated by iteration of the anisotropic *g*-values, (super)hyperfine coupling constants and line widths using the W95EPR program (obtained from Prof. Frank Neese, the University of Bonn).

Computational Details. The geometries of **1**, $\mathbf{1}^{\bullet-}$, **3**, $\mathbf{3}^{\bullet-}$, **3**-dppv, and **3**-dppv$^{\bullet-}$, were optimized with Turbomole 6.4 program[29] using the BP86[30−32] functional and the def2-TZVP[33] basis set. These calculations also yielded the frontier orbitals and spin density plots EPR parameters[34] were subsequently calculated with ORCA,[35] using the coordinates from the structures optimized in Turbomole as input. In the Orca calculations, we used Ahlrich's def2-TZVP[33] basis set and the B3LYP functional.[36]

■ ASSOCIATED CONTENT

Ⓢ Supporting Information

Details on X-ray crystal analyses of **L**, **3**, and **3**-dppv, as well as results for chemical reduction of complex **3**, DFT calculations, spectroscopic and electrochemical analyses. This material is available free of charge via the Internet at http://pubs.acs.org.

■ AUTHOR INFORMATION

Corresponding Authors

*E-mail: f.hartl@reading.ac.uk. (F.H.)
*E-mail: s.woutersen@uva.nl. (S.W.)
*E-mail: j.n.h.reek@uva.nl. (J.N.H.R.)

Author Contributions

⊥P.L. and S.A. contributed equally to this work.

Notes

The authors declare no competing financial interests.

■ ACKNOWLEDGMENTS

We are grateful to The Netherlands' Organization for Scientific Research (NWO−CW; ECHO Grant No. 700.57.042; F.H. and J.N.H.R.) and the German National Academy of Sciences (Leopoldina research fellowship, Grant No. LPDS 2011-18; S.A.) for financial support. Helpful discussions with Dr. Volodymyr Lyaskovskyy, Mr. Hungcheng Chen, and Dr. René Williams (University of Amsterdam) are acknowledged.

■ REFERENCES

(1) (a) Tard, C.; Liu, X.; Ibrahim, S. K.; Bruschi, M.; Gioia, L. D.; Davies, S. C.; Yang, X.; Wang, L.-S.; Sawers, G.; Pickett, C. J. *Nature* **2005**, *433*, 610−613. (b) Tard, C.; Pickett, C. J. *Chem. Rev.* **2009**, *19*, 2245−2274. (c) Gloaguen, F.; Rauchfuss, T. B. *Chem. Soc. Rev.* **2009**, *38*, 100−108. (d) Capon, J.-F.; Gloaguen, F.; Pétillon, F. Y.; Schollhammer, P.; Talarmin, J. *Coord. Chem. Rev.* **2009**, *253*, 1476−1494.

(2) Peters, J. W.; Lanzilotta, W. N.; Lemon, B. J.; Seefeldt, L. C. *Science* **1998**, *282*, 1853−1858.

(3) (a) Gloaguen, F.; Lawrence, J. D.; Rauchfuss, T. B. *J. Am. Chem. Soc.* **2001**, *123*, 9476−9477. (b) Chong, D.; Georgakaki, I. P.; Mejia-Rodriguez, R.; Sanabria-Chinchilla, J.; Soriaga, M. P.; Darensbourg, M. Y. *Dalton Trans.* **2003**, 4158−4163. (c) Capton, J.-F.; Gloaguen, F.; Schollhammer, P.; Talarmin, J. *J. Electroanal. Chem.* **2004**, *566*, 241−247. (d) Duan, L.; Wang, M.; Li, P.; Na, Y.; Wang, N.; Sun, L. *Dalton Trans.* **2007**, 1277−1283. (e) Nann, T.; Ibrahim, S. K.; Woi, P.-M.; Xu, S.; Ziegler, J.; Pickett, C. J. *Angew. Chem., Int. Ed.* **2010**, *49*, 1574−1577.

(4) (a) Lomoth, R.; Ott, S. *Dalton Trans.* **2009**, 9952−9959. (b) Wang, M.; Chen, L.; Li, X.; Sun, L. *Dalton Trans.* **2011**, *40*, 12793−12800. (c) Wang, F.; Wang, W.-G.; Wang, H.-Y.; Si, G.; Tung, C.-H.; Wu, L.-Z. *ACS Catal.* **2012**, *2*, 407−416. (d) Streich, D.; Astuti, Y.; Orlandi, M.; Schwartz, L.; Lomoth, R.; Hammarström, L.; Ott, S. *Chem.—Eur. J.* **2010**, *16*, 60−63. (e) Yu, T.; Zeng, Y.; Chen, J.; Li, Y.-Y.; Yang, G.; Li, Y. *Angew. Chem., Int. Ed.* **2013**, *52*, 5631−5635.

(5) (a) Ott, S.; Kritikos, M.; Åkermark, B.; Sun, L. *Angew. Chem., Int. Ed.* **2003**, *42*, 3285−3288. (b) Wolpher, H.; Borgström, M.; Hammarström, L.; Bergquist, J.; Sundström, V.; Styring, S.; Sun, L.; Åkermark, B. *Inorg. Chem. Commun.* **2003**, 989−991. (c) Ott, S.; Borgström, M.; Kritikos, M.; Lomoth, R.; Bergquist, J.; Åkermark, B.; Hammarstrom, L.; Sun, L. *Inorg. Chem.* **2004**, *43*, 4683−4692.

(6) Sun, L.; Åkermark, B.; Ott, S. *Coord. Chem. Rev.* **2005**, *249*, 1653−1663.

(7) Ekström, J.; Abrahamsson, M.; Olson, C.; Bergquist, J.; Kaynak, F. B.; Eriksson, L.; Sun, L.; Becker, H.-C.; Åkermark, B.; Hammarström, L.; Ott, S. *Dalton Trans.* **2006**, 4599−4606.

(8) Na, Y.; Pan, J.; Wang, M.; Sun, L. *Inorg. Chem.* **2007**, *46*, 3813−3815.

(9) Li, X.; Wang, M.; Chen, L.; Wang, X.; Dong, J.; Sun, L. *ChemSusChem* **2012**, *5*, 913−919.

(10) Song, L.-C.; Tang, M.-Y.; Mei, S.-Z.; Huang, J.-H.; Hu, Q.-M. *Organometallics* **2007**, *26*, 1575−1577.

(11) Li, X.; Wang, M.; Zhang, S.; Pan, J.; Na, Y.; Liu, J.; Åkermark, B.; Sun, L. *J. Phys. Chem. B* **2008**, *112*, 8198−8202.

(12) Kluwer, A. M.; Kapre, R.; Hartl, F.; Lutz, M.; Spek, A. L.; Brouwer, A. M.; van Leeuwen, P. W. N. M.; Reek, J. N. H. *Proc. Natl. Acad. Sci. U.S.A.* **2009**, *106*, 10460−10465.

(13) (a) Samuel, A. P. S.; Co, D. T.; Stern, C. L.; Wasielewski, M. R. *J. Am. Chem. Soc.* **2010**, *132*, 8813−8815. (b) Poddutoori, P.; Co, D. T.; Samuel, A. P. S.; Kim, C. H.; Vagnini, M. T.; Wasielewski, M. R. *Energy Environ. Sci.* **2011**, *4*, 2441−2450.

(14) Wright, R. J.; Lim, C.; Tilley, T. Don *Chem.—Eur. J.* **2009**, *15*, 8518−8525.

(15) (a) Best, S. P. *Coord. Chem. Rev.* **2005**, *249*, 1536−1554. (b) Borg, S. J.; Behrsing, T.; Best, S. P.; Razavet, M.; Liu, X.; Pickett, C. J. *J. Am. Chem. Soc.* **2004**, *126*, 16988−16999. (c) Tschierlei, S.; Ott, S.; Lomoth, R. *Energy Environ. Sci.* **2011**, *4*, 2340−2352.

(16) Jablonskytė, A.; Wright, J. A.; Fairhurst, S. A.; Peck, J. N. T.; Ibrahim, S. K.; Oganesyan, V. S.; Pickett, C. J. *J. Am. Chem. Soc.* **2011**, *133*, 18606−18909.
(17) (a) Bingaman, J. L.; Kohnhorst, C. L.; Van Meter, G. A.; McElroy, B. A.; Rakowski, E. A.; Caplins, B. W.; Gutowski, T. A.; Stromberg, C. J.; Webster, C. E.; Heiweil, E. J. *J. Phys. Chem. A* **2012**, *116*, 7261−7271. (b) Johnson, M.; Thuman, J.; Letterman, R. G.; Stromberg, C. J.; Webster, C. E.; Heilweil, E. J. *J. Phys. Chem. B* **2013**, *117*, 15792−15803.
(18) (a) Stewart, A. I.; Clark, I. P.; Ibrahim, S. K.; Parker, A. W.; Pickett, C. J.; Hunt, N. T. *J. Phys. Chem. B* **2008**, *112*, 10023−10032. (b) Stewart, A. I.; Wright, J. A.; Greetham, G. M.; Kaziannis, S.; Santabarbara, S.; Towrie, M.; Parker, A. W.; Pickett, C. J.; Hunt, N. T. *Inorg. Chem.* **2010**, *49*, 9563−9573. (c) Kaziannis, S.; Santabarbara, S.; Wright, J. A.; Greetham, G. M.; Towrie, M.; Parker, A. W.; Pickett, C. J.; Hunt, N. T. *J. Phys. Chem. B* **2010**, *114*, 15370−15379.
(19) Singh, P. S.; Rudbeck, H. C.; Huang, P.; Ezzaher, S.; Eriksson, L.; Stein, M.; Ott, S.; Lomoth, R. *Inorg. Chem.* **2009**, *48*, 10883−10885.
(20) Hall, G. B.; Chen, J.; Mebi, C. A.; Okumura, N.; Swenson, M. T.; Ossowski, S. E.; Zakai, U. I.; Nichol, G. S.; Lichtenberger, D. L.; Evans, D. H.; Glass, R. S. *Organometallics* **2013**, *32*, 6605−6612.
(21) Liu, Y.-C.; Yen, T.-H.; Tseng, Y.-J.; Hu, C.-H.; Lee, G.-H.; Chiang, M.-H. *Inorg. Chem.* **2012**, *51*, 5997−5999.
(22) Connelly, N. G.; Geiger, W. E. *Chem. Rev.* **1996**, *96*, 877−910.
(23) Justice, A. K.; Zampella, G.; Gioia, L. D.; Rauchfuss, T. B.; van der Vlugt, J. I.; Wilson, S. R. *Inorg. Chem.* **2007**, *46*, 1655−1664.
(24) Li, P.; Wang, M.; He, C.; Li, G.; Liu, X.; Chen, C.; Åkermark, B.; Sun, L. *Eur. J. Inorg. Chem.* **2005**, 2506−2513.
(25) (a) Nocera, D. G.; Teets, T. S. *Chem. Commun.* **2011**, *47*, 9268−9274. (b) Artero, V.; Chavarot-Kerlidou, M.; Fontecave, M. *Angew. Chem., Int. Ed.* **2011**, *50*, 7238−7266. (c) Du, P.; Eisenberg, R. *Energy Environ. Sci.* **2012**, *5*, 6012−6021.
(26) Tesmer, M.; Vahrenkamp, H. *Eur. J. Inorg. Chem.* **2001**, 1183−1188.
(27) Krejčík, M.; Daněk, M.; Hartl, F. *J. Electroanal. Chem.* **1991**, *317*, 179−187.
(28) Meuzelaar, H.; Marino, K. A.; Huerta-Viga, A.; Panman, M. R.; Smeenk, L. E. J.; Kettelarij, A. J.; van Maarseveen, J. H.; Timmerman, P.; Bolhuis, P. G.; Woutersen, S. *J. Phys. Chem. B* **2013**, *117*, 11490−11501.
(29) Ahlrichs, R.; Bär, M.; Barton, H.-P.; Bauernschmitt, R.; Böcher, S.; Rhrig, M.; Eichkorn, K.; Elliott, S.; Furche, F.; Haase, F.; M. Häser, C. Hättig, Horn, H.; Huber, C.; Huniar, U.; Kattannek, M.; A. Köhn, C. Kölmel, Kollwitz, M.; May, K.; Ochsenfeld, C.; H. Öhm, A. Schäfer, Schneider, U.; Treutler, O.; Tsereteli, K.; Unterreiner, B.; von Arnim, M.; Weigend, F.; Weis, P.; Weiss, H. *Turbomole,* Version 6.4; University of Karlsruhe: Karlruhe, Germany, January 2002.
(30) Becke, A. D. *Phys. Rev. A* **1988**, *38*, 3098−3110.
(31) Perdew, J. P. *Phys. Rev. B* **1986**, *33*, 8822−8824.
(32) Perdew, J. P. *Phys. Rev. B* **1986**, *34*, 7406−7406.
(33) Weigend, F.; Ahlrichs, R. *Phys. Chem. Chem. Phys.* **2005**, *7*, 3297−3305.
(34) Some references and reviews on DFT approaches to EPR parameters: (a) van Lenthe, E.; van der Avoird, A.; Wormer, P. E. S. *J. Chem. Phys.* **1997**, *107*, 2488−2498. (b) van Lenthe, E.; van der Avoird, A.; Wormer, P. E. S. *J. Chem. Phys.* **1998**, *108*, 4783−4796. (c) Neese, F. *Curr. Opin. Chem. Biol.* **2003**, *7*, 125−135. (d) Neese, F.; Solomon, E. *In Magnetoscience—From Molecules to Materials;* Miller, J. S.; Drillon, M., Eds.; Wiley: New York, 2003; pp 345−466. (e) Peng, G.; Nichols, J.; McCullough, E. A.; Spence, J. *Inorg. Chem.* **1994**, *33*, 2857−2864.
(35) Neese, F. *ORCA—An ab initio, Density Functional and Semiempirical program package*, Version 2.9; Max Planck Institute for Chemical Energy Conversion: Mulheim an der Ruhr, Germany, 2010.
(36) (a) Lee, C.; Yang, W.; Parr, R. G. *Phys. Rev. B* **1998**, *37*, 785−789. (b) Becke, A. D. *J. Chem. Phys.* **1993**, *98*, 1372−1377. (c) Becke, A. D. *J. Chem. Phys.* **1993**, *98*, 5648−5652.